

Dual Projection Generative Adversarial Networks for Conditional Image Generation

Ligong Han,¹ Martin Renqiang Min,² Anastasis Stathopoulos,¹
 Yu Tian,¹ Ruijiang Gao,³ Asim Kadav,² Dimitris Metaxas¹

¹Department of Computer Science, Rutgers University ²NEC Labs America

³McCombs School of Business, The University of Texas at Austin

lh599@rutgers.edu, renqiang@nec-labs.com, as2947@cs.rutgers.edu

yt219@cs.rutgers.edu, ruijiang@utexas.edu, asim@nec-labs.com, dnm@cs.rutgers.edu

Abstract

Conditional Generative Adversarial Networks (cGANs) extend the standard unconditional GAN framework to learning joint data-label distributions from samples, and have been established as powerful generative models capable of generating high-fidelity imagery. A challenge of training such a model lies in properly infusing class information into its generator and discriminator. For the discriminator, class conditioning can be achieved by either (1) directly incorporating labels as input or (2) involving labels in an auxiliary classification loss. In this paper, we show that the former directly aligns the class-conditioned fake-and-real data distributions $P(\text{image}|\text{class})$ (data matching), while the latter aligns data-conditioned class distributions $P(\text{class}|\text{image})$ (label matching). Although class separability does not directly translate to sample quality and becomes a burden if classification itself is intrinsically difficult, the discriminator cannot provide useful guidance for the generator if features of distinct classes are mapped to the same point and thus become inseparable. Motivated by this intuition, we propose a Dual Projection GAN (P2GAN) model that learns to balance between data matching and label matching. We then propose an improved cGAN model with Auxiliary Classification that directly aligns the fake and real conditionals $P(\text{class}|\text{image})$ by minimizing their f -divergence. Experiments on a synthetic Mixture of Gaussian (MoG) dataset and a variety of real-world datasets including CIFAR100, ImageNet, and VGGFace2 demonstrate the efficacy of our proposed models.

1. Introduction

Generative Adversarial Networks (GANs) [7] are an algorithmic framework that allows implicit generative modeling of data distribution from samples [31]. It has at-

tracted great attention due to its ability to model very high-dimensional data, such as images or videos and to produce sharp and faithful samples [16, 45, 3]. Conditional GAN (cGAN) [27, 35, 30] is an extension of GAN that utilizes the label information and aims to learn the joint distribution of data and label. Thanks to its ability to control over the generative process by conditioning on labels, it has been widely adopted in real-world problems including class-conditional image generation [33, 35, 5], text-to-image generation [38, 46], image-to-image generation [14, 47], text-to-video synthesis [23, 1, 10, 9], domain adaptation [13, 28] etc.

Different conditional GANs differ in the way how data and labels are incorporated in the discriminator. Class conditioning can be achieved by either (1) conditioning the discriminator directly on labels or their embeddings [27, 14, 30], or by (2) incorporating an auxiliary classification loss in the objective, as in (T)AC-GANs[27, 6]. Recently, cGAN has received a major update that changed the label from being concatenated [27, 38, 46] to being projected [30]. The projection discriminator takes the inner product between the label embedding and the data/image embedding, and remains to be the choice of many state-of-the-art methods [45, 3].

In this paper, we first give insights on projection discriminators. We point out that the success of projection can be explained by its flexible form. By tying real and fake class embeddings as their difference, a projection discriminator can ideally realize two extremes in a single form: (1) matching conditional label distributions $P(\text{class}|\text{image})$ (*label matching*), and (2) matching conditional data distributions $P(\text{image}|\text{class})$ (*data matching*). Moreover, the visualization of data embeddings of trained projection discriminators does not show obvious patterns of class clustering. This suggests that projection may bias towards conditional data matching. Although label matching does not

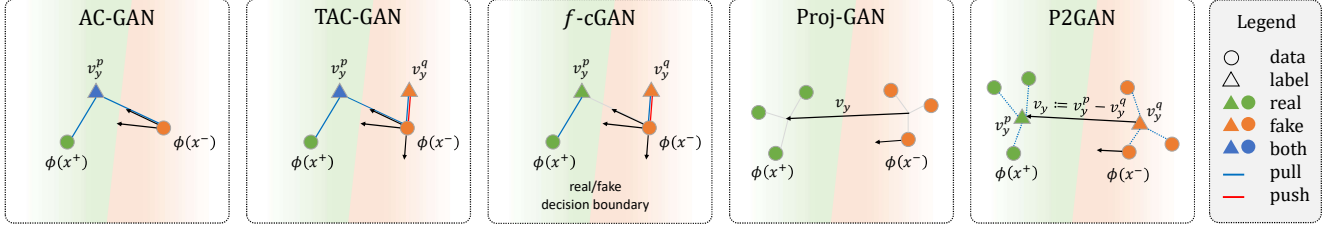


Figure 1: Illustrative figures visualize the learning schema of conditional discriminator losses. The color indicates how real/fake embeddings interact during *discriminator training*. The green/red boundary indicates (unconditional) real/fake decision boundary. Triangles represent class embeddings, and circles indicate image embeddings (e.g. v_y^p is blue triangle in AC-GAN since it is class embedding and is trained on both real and fake data). Solid blue and red lines represent pull/push forces respectively. Black arrows indicate the forces that a fake image embedding receives.

directly translate to the fidelity of generated samples, it is still desirable for generating high-quality images. For example, the discriminator would not provide useful guidance for the generator if features of distinct classes are mapped to the same point and thus become inseparable.

To this end, we propose a new conditional generative adversarial network, namely *Dual Projection GAN* (P2GAN). The main feature of our design is to inherit the flexibility of projection while performing explicit label matching. Realized by auxiliary classification losses, label matching enables the discriminator to exploit useful information for the generator. However, if such task is intrinsically difficult (such as ImageNet [39]), label matching becomes a burden. In an extreme case when the auxiliary classification task failed completely, (T)AC-GANs will degrade to an unconditional GAN while P2GAN degrades to a projection GAN. We also present adaptive approaches to weighing data matching and label matching. Furthermore, we respectively propose two variants for explicit data matching and label matching: (1) direct data matching GAN (DM-GAN), (2) and f -cGAN which aligns the fake and real conditionals $P(\text{class}|\text{image})$ by minimizing their f -divergence. Finally, we conduct extensive experiments on various datasets to show the efficacy of the proposed models.

2. Related Work

Projection. The key idea of Proj-GAN is to tie parameters of AC and twin AC. This design brings flexibility in modeling data matching and label matching. We leverage its flexible design in our P2GAN model. The same projection form is considered in projection-based MINE [2, 11].

Multi-task learning. Training GANs with both discrimination loss and classification loss can be viewed as a multi-task learning problem. [18] propose a principled approach [18] that weighs multiple loss functions by considering the homoscedastic uncertainty of each task. The proposed P2GAN-w model is built upon this notion.

f -divergence in GANs. [34] formulated a family of

GANs into a variational f -divergence minimization framework [34]. Their proposed f -GAN is for marginal matching (unconditional GAN) while our f -cGAN aims to minimize the f -divergence between real and fake conditionals and does not optimize its dual form.

Twin auxiliary classifiers. TAC-GAN corrects the bias in AC-GANs by introducing a twin AC and maximizing its classification loss on generated samples. A binary version of twin AC has been introduced as an Anti-Labeler in CausalGAN [20]. CausalGAN has observed unstable training behavior after introducing such binary twin ACs. RoboGAN [25] splits the categorical classification losses of real and fake data in AC-GAN, however, it does not have a twin AC (dual projections) and does not aim to balance label-matching and data-matching.

3. Method

3.1. Background

Throughout the paper, we denote data-label pairs as $\{x_i, y_i\}_{i=1}^n \subseteq \mathcal{X} \times \mathcal{Y}$ drawn from the joint distribution P_{XY} , where x is an image (or other forms of data) and y is its label, *i.e.*, $\mathcal{Y} = \{1, \dots, K\}$. A generator is trained to transform samples $z \sim P_Z$ from a canonical distribution conditioned on labels to match the real data distributions. *Real* distributions are denoted as P and *generated* distributions are denoted as Q . We also denote real and fake data as $x^+ \sim P_X$ and $x^- \sim Q_X$, respectively. The discriminator of a conditional GAN learns to distinguish samples drawn from the joint distribution P_{XY} and Q_{XY} . Its objectives can be written as:

$$L_D = \mathbb{E}_{x, y \sim P_{XY}} \mathcal{A}(-\tilde{D}(x, y)) + \quad (1)$$

$$\mathbb{E}_{z \sim P_Z, y \sim Q_Y} \mathcal{A}(\tilde{D}(G(z, y), y)), \quad \text{and}$$

$$L_G = \mathbb{E}_{z \sim P_Z, y \sim Q_Y} \mathcal{A}(-\tilde{D}(G(z, y), y)). \quad (2)$$

Here \mathcal{A} is the *activation function* and \tilde{D} is the *logit* or discriminator's output before activation. Note that choosing

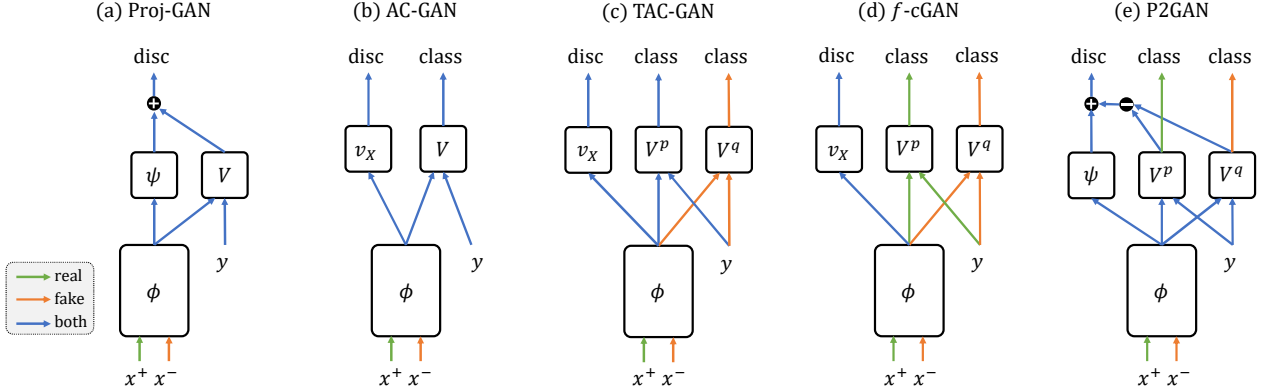


Figure 2: Discriminator models for conditional GANs. Solid green lines represent the flow path of real data, red line represent the flow path of generated data and blue lines mean both real and generated data flow through them. x^+ represents real images, x^- are generated images and y are labels. Matrix V^p and V^q are the collection of class embeddings $\{v_y^p\}$ and $\{v_y^q\}$ for twin auxiliary classifiers, respectively.

$\mathcal{A}(t) = \text{softplus}(t) = \log(1 + \exp(t))$ recovers the original GAN formulation[7]. With this activation function, the logit of an optimal discriminator in Equation 1 can be decomposed in two ways,

$$\tilde{D}^*(x, y) = \underbrace{\log \frac{P(x)}{Q(x)}}_{\text{Marginal Matching}} + \underbrace{\log \frac{P(y|x)}{Q(y|x)}}_{\text{Label Matching}} \quad (3)$$

$$= \underbrace{\log \frac{P(x|y)}{Q(x|y)}}_{\text{Data Matching}} + \log \frac{P(y)}{Q(y)}. \quad (4)$$

From Equation 3, one can derive the logit of a *projection* discriminator [30],

$$\tilde{D}(x, y) = v_y^T \phi(x) + \psi(\phi(x)), \quad (5)$$

where $\phi(\cdot)$ is the image embedding function, v_y is embedding of class y , and ψ collects the residual terms. $v_y := v_y^p - v_y^q$ is the difference of real and fake class embeddings.

3.2. Projection and Dual Projection GANs

Effectiveness of tying class embeddings. The key idea of a projection discriminator [30] is to tie the parameters v_y^p and v_y^q into a single v_y . Intuitively, tying embeddings allows a projection discriminator to turn the problem of learning categorical decision boundaries to learning a relative translation vector for each class. The latter is much easier than the former. Intuitively, it is in general easier to learn a relative comparison than to learn each parameter in an absolute scale. For example, learning v_y^p is a hard problem by itself when training on large scale datasets like ImageNet [39].

Without loss of generality, let's assume $\psi(\cdot)$ as a linear function v_ψ . From Equation 1 we can see that L_D is trying to maximize $(v_y + v_\psi)^T \phi(x^+)$ and to minimize

$(v_y + v_\psi)^T \phi(x^-)$. If we approximate *softplus* function by *ReLU* = $\max(0, \cdot)$, we observe that the loss is large when x^+ and x^- are mis-classified, under which $L_D \approx (v_y + v_\psi)^T (\phi(x^-) - \phi(x^+))$. Intuitively, the learning procedure of Proj-GAN can be understood as performing two alternative steps,

D-step : Align $(v_y + v_\psi)$ with $(\phi(x^+) - \phi(x^-))$;
 G-step : Move $\phi(x^-)$ along $(v_y + v_\psi)$.

This shows that by tying parameters, Proj-GAN is able to directly perform *data matching* (align $Q(x|y)$ with $P(x|y)$) without explicitly enforcing *label matching*.

Enforcing label matching. Ideally, v_y should recover the difference between underlying v_y^p and v_y^q , but there is no explicit constraint to enforce such property. To do this, we start by untying the class embeddings $v_y := v_y^p - v_y^q$. Then, we encourage V^p and V^q to learn conditional distributions $p(y|x)$ and $q(y|x)$, respectively*. This is usually done by minimizing cross-entropy losses with a *softmax* function,

$$L_{mi}^p = -v_y^{pT} \phi(x^+) + \log \sum_{y'} \exp(v_{y'}^{pT} \phi(x^+)), \text{ and} \\ L_{mi}^q = -v_y^{qT} \phi(x^-) + \log \sum_{y'} \exp(v_{y'}^{qT} \phi(x^-)). \quad (6)$$

Note that the two classifiers V^p and V^q are trained on real and fake data respectively. This is different from AC-GAN and TAC-GAN where the (first) discriminator is trained on both x^+ and x^- . This is shown in Figure 1 and 2.

Dual Projection GAN (P2GAN). The discriminator and

*Matrix V is the collection of class embeddings v_y for all categories.

generator losses for P2GAN is given as follows,

$$L_D^{P2} = L_D(\tilde{D}) + L_{mi}^p + L_{mi}^q, \quad (7)$$

and $L_G^{P2} = L_G(\tilde{D})$,

$$\text{with } \tilde{D} = (v_y^p - v_y^q)^\top \phi(x) + \psi(\phi(x))$$

The proposed method has untied projection vectors, thus we term the model Dual Projection GAN, or P2GAN. Note that both $L_D(\tilde{D})$ and L_{mi}^p contain parameter V^p , and similarly, both $L_D(\tilde{D})$ and L_{mi}^q contain parameter V^q . It is also worth mentioning that similar to the Proj-GAN, P2GAN only proposes a form of the logit while leaves the activation function free of choices.

We observe that when cross-entropy losses are removed, P2GAN is equivalent to Proj-GAN except that v_y is over-parameterized as $v_y^p - v_y^q$. This suggests that when class separability is intrinsically difficult to model and the two cross-entropy losses are not effectively optimized, P2GAN reduces to a Proj-GAN. In this case, a model that relies on *marginal-conditional* [22] decomposition, such as an AC-GAN or a TAC-GAN, degrades to an unconditional GAN instead. This illustrates that the proposed P2GAN *implicitly* balances data matching and label matching by inheriting the Proj-GAN. We can also *explicitly* weigh L_{mi}^p and L_{mi}^q .

Weighted Dual Projection GAN (P2GAN-w). From a multi-task learning perspective [18], it should be beneficial to let the model learn to weigh *data matching* and *label matching*. Here we consider adding a “gate” between the two losses,

$$L_D^{P2w} = L_D + \lambda \cdot (L_{mi}^p + L_{mi}^q). \quad (8)$$

We tested three variants of weighted P2GAN: (1) exponential decay, (2) scalar valued, and (3) amortised.

P2GAN-d. The simplest way is to define λ as a decaying factor. We set $\lambda = e^{-t/T}$, t is the number of iterations during training time.

P2GAN-s. Let $\lambda \geq 0$ be a learnable parameter and initialized as 1. When $\lambda = 0$, P2GAN-s reduces to a Proj-GAN. When $\lambda > 0$, class separation is explicitly enforced. The data matching task is intuitively much easier than the label matching task in the early stage of training and λ would quickly vanish. To accommodate this, we follow [18] and add a penalty term on λ (P2GAN-sp),

$$L_D^{P2sp} = L_D + \lambda \cdot (L_{mi}^p + L_{mi}^q) - \frac{1}{2} \log \lambda. \quad (9)$$

P2GAN-a. We also experimented with learning amortized homoscedastic weights for each data point. $\lambda(x) \geq 0$ is then a function of x (P2GAN-a). Since $\lambda(x)$ are per-sample weights, in Equation 8 it should be inside of the expectation. We defer its lengthy definition in Supplementary. Likewise, a penalty term can be added (P2GAN-ap). Also, when loss

terms involve non-linearity in the mini-batch expectation, for example, the log in MINE [2], any type of “linearization” tricks can be applied [32].

Comparisons of different weighting strategies are given in experiments Table 1. In practice we find $\lambda(x)$ with penalty works best. In following Experiments, P2GAN-w stands for P2GAN-ap, if not specified.

3.3. Theoretical Analysis

As discussed previously, a projection discriminator defined in Equation 5 can flexibly transit between two decomposition forms. Here we discuss two variants of conditional GAN models that perform *only* data matching or label matching.

cGAN that performs data matching (DM-GAN). Setting $\psi(\cdot)$ as zero[†], Proj-GAN can be viewed as a weighted sum of K unconditional GAN objectives with binary cross-entropy losses (where K is the number of classes):

Proposition 1. *When $\psi = 0$, a Proj-GAN reduces to K unconditional GANs, each of them minimizes the Jensen-Shannon divergence between $P_{X|y}$ and $Q_{X|y}$ with mixing ratio $\{\frac{P(y)}{P(y)+Q(y)}, \frac{Q(y)}{P(y)+Q(y)}\}$. Its value function can be written as,*

$$\mathbb{E}_{P_Y} \left\{ \mathbb{E}_{P_{X|Y}} \log D(x|y) + \frac{Q_y}{P_y} \mathbb{E}_{Q_{X|Y}} \log (1 - D(x|y)) \right\}.$$

We observe a slight improvement in terms of FID score from our early experiment on CIFAR100[‡], which might suggest that Proj-GAN biases towards data matching than label matching. DM-GAN is also the cGAN implementation in [26, 17].

cGAN that performs label matching (f -cGAN). At the other end of the spectrum, if we explicitly model the marginal matching and label matching terms in Equation 3, we arrive at a (T)AC-GAN-like model which follows the *marginal-conditional* decomposition. To be precise, marginal matching can be achieved via (unconditional) GAN loss, and label matching can be enforced by minimizing their divergence.

Proposition 2. *Given a generator G , if cross entropy losses L_{mi}^p and L_{mi}^q are minimized optimally, then the difference of two losses evaluated at fake data equals the reverse KL-divergence between $P_{Y|X}$ and $Q_{Y|X}$,*

$$L_{mi}^p(x^-) - L_{mi}^q(x^-) = \mathbb{E}_{Q_X} KL(Q_{Y|X} \| P_{Y|X}). \quad (10)$$

[†]In practice spectral normalization [29] is often applied and this null solution for ψ cannot be reached.

[‡]this conclusion is not reflected in Table 7 due to different hyper-parameters and configurations.

From the above proposition we derive a new conditional GAN,

$$\begin{aligned} L_D^f &= L_D(\tilde{D}) + L_{mi}^p(x^+) + L_{mi}^q(x^-), \\ \text{and } L_G^f &= L_G(\tilde{D}) + L_{mi}^p(x^-) - L_{mi}^q(x^-), \\ \text{with } \tilde{D} &= v_X^T \phi(x) + b \end{aligned} \quad (11)$$

In fact, $L_{mi}^p(x^-) - L_{mi}^q(x^-) = \mathbb{E}_{Q_{XY}} - \log \frac{Q^p(y|x)}{Q^q(y|x)}$. By replacing the $-\log$ with function f , we can also generalize the reverse-KL to f -divergence [34], $\mathbb{E}_{Q_{XY}} f\left(\frac{P(y|x)}{Q(y|x)}\right) = \mathbb{E}_{Q_X} D_f(P_{Y|X} \| Q_{Y|X})$. The generator loss then becomes

$$L_G^f = L_G + \mathbb{E}_{Q_{XY}} f(\exp(T^p(x, y) - T^q(x, y))). \quad (12)$$

Here, $T^p = v_y^{pT} \phi(x) - \log \sum_{y'} \exp(v_{y'}^{pT} \phi(x))$ is an estimator of $\log P(y|x)$, and similarly T^q is an estimator of $\log Q(y|x)$. Equation 11 and 12 defines a general conditional GAN framework, which we call f -cGAN.

To show that f -cGAN is theoretically sound and Nash equilibrium can be achieved, we provide the following theorem.

Theorem 1. Denoting P_{XY} and Q_{XY} as the data distribution and the distribution induced by G , their Jensen-Shannon divergence is upper bounded by the following,

$$\begin{aligned} JSD(P_{XY}, Q_{XY}) &\leq \quad (13) \\ 2c_1 \sqrt{2JSD(P_X, Q_X)} + c_2 \sqrt{2KL(P_{Y|X} \| Q_{Y|X}^p)} + \\ c_2 \sqrt{2KL(Q_{Y|X} \| Q_{Y|X}^q)} + c_2 \sqrt{2KL(Q_{Y|X}^q \| Q_{Y|X}^p)}. \end{aligned}$$

in the above, constants c_1 and c_2 are upper bounds of $\frac{1}{2} \int |P_{Y|X}(y|x)|\mu(x, y)$ and $\int |Q_X(x)|\mu(x)$, respectively, where μ is a σ -finite measure.

3.4. Comparison with Other Methods

First, dual projection GAN extends a projection GAN by untying class embeddings and enforcing class separability in each domain. Comparing P2GAN with f -cGAN, both of them minimizes $L_{mi}^p(x^+) + L_{mi}^q(x^-)$ in the discriminator loss. As for the generator loss, f -cGAN minimizes $L_{mi}^p(x^-) - L_{mi}^q(x^-)$, while P2GAN enforces label matching via $L_G((v_y^p - v_y^q)^T \phi(x^-) + \psi(\phi(x^-)))$ thus the *LogSumExp* function is not involved.

By adding a term $L_{mi}^p(x^-)$ to L_D^f in Equation 11, one can recover the TAC-GAN⁸. It is worth noting that this term is required since TAC-GAN aims to chain $\mathbb{E}_{P_X} \text{KL}(P_{Y|X} \| Q_{Y|X}^p)$ and $\mathbb{E}_{Q_X} \text{KL}(Q_{Y|X} \| Q_{Y|X}^p)$

⁸Note that this term is already omitted in its actual implementation, however, it is indispensable for the theoretical analysis to hold.

together, while our f -cGAN tries directly align $Q_{Y|X}$ with $P_{Y|X}$. In experiments we show that this simple trick can largely boost performance. Further, by removing all terms related to L_{mi}^q we derive AC-GAN.

Both P2GAN and f -cGAN only model *data-to-class* relations, and *data-to-data* relation is indirectly modeled via class embeddings. While ContraGAN [15] models these two relations directly. It is orthogonal to our method and we leave it for future work.

Table 1: FID scores of different weighting strategies for P2GAN-w. All models are trained for 80000 iterations on ImageNet, 62000 iterations on CIFAR100, and 50000 iterations on VGGFace200.

| Datasets | ImageNet | CIFAR100 | VGGFace200 |
|------------------|--------------|-------------|--------------|
| P2GAN | 19.22 | 10.55 | 23.15 |
| P2GAN-d (T=200) | - | 10.51 | 21.24 |
| P2GAN-d (T=2000) | - | 10.35 | 24.49 |
| P2GAN-s | 18.62 | 9.03 | 20.59 |
| P2GAN-sp | 20.68 | 9.51 | 20.18 |
| P2GAN-a | - | 10.13 | 20.26 |
| P2GAN-ap | 18.31 | 9.82 | 18.99 |

Table 2: Average rank of Proj-GAN, TAC-GAN, f -cGAN and P2GAN on MoG dataset. For each method, the average ranks of using BCE loss, hinge loss, and all experiments are reported.

| Models | Proj-GAN | TAC-GAN* | f -cGAN (ours) | P2GAN (ours) |
|---------|-------------|----------|------------------|--------------|
| BCE | 3.90 | 2.45 | 2.15 | 1.50 |
| Hinge | 1.80 | 3.35 | 2.45 | 2.40 |
| Overall | 2.85 | 2.90 | 2.30 | 1.95 |

Table 3: Max-FID scores for 1D MOG synthetic dataset.

| BCE / Hinge | $d_m = 1$ | $d_m = 2$ | $d_m = 3$ | $d_m = 4$ | $d_m = 5$ |
|-------------|---------------|---------------|---------------|---------------|---------------|
| Proj-GAN | 0.0059 | 0.0213 | 0.0291 | 0.0339 | 0.0796 |
| TAC-GAN* | 0.0029 | 0.0090 | 0.0134 | 0.0169 | 0.0243 |
| f -cGAN | 0.0032 | 0.0072 | 0.0129 | 0.0184 | 0.0213 |
| P2GAN | 0.0026 | 0.0060 | 0.0085 | 0.0124 | 0.0212 |
| Proj-GAN | 0.0200 | 0.0481 | 0.0733 | 0.1253 | 0.2066 |
| TAC-GAN* | 0.0270 | 0.0887 | 0.1307 | 0.1483 | 0.2285 |
| f -cGAN | 0.0236 | 0.0829 | 0.1187 | 0.0847 | 0.1100 |
| P2GAN | 0.0245 | 0.0473 | 0.0901 | 0.1076 | 0.1698 |

4. Experiments

Datasets. In this section, we first show experimental results for model analysis on an imbalanced subset of CIFAR100 [21] (denoted as CIFAR100IB). Then we then report results of different baselines across various datasets. Finally, ablation studies are presented. We evaluate the distribution matching ability of different models on a synthetic

Table 4: Inception Scores (IS), Fréchet Inception Distances (FID) and the maximum intra FID (max-FID). Our proposed adaptive P2GAN achieves the highest IS, lowest FID and lowest max-FID in most cases. The top-two best performing methods are marked in boldface.

| | Proj-GAN | | | TAC-GAN* | | | f-cGAN (ours) | | | P2GAN (ours) | | | P2GAN-w (ours) | | |
|--------------|-----------------------------------|------------------|----------------------|-----------------------------------|------------------|----------------------|-------------------|------------------|----------------------|-------------------------------------|------------------|----------------------|-------------------------------------|------------------|----------------------|
| | IS \uparrow | FID \downarrow | max-FID \downarrow | IS \uparrow | FID \downarrow | max-FID \downarrow | IS \uparrow | FID \downarrow | max-FID \downarrow | IS \uparrow | FID \downarrow | max-FID \downarrow | IS \uparrow | FID \downarrow | max-FID \downarrow |
| CIFAR100 | 9.17 \pm 0.14 | 9.98 | 186.46 | 8.86 \pm 0.12 | 9.63 | 223.24 | 8.41 \pm 0.09 | 10.76 | 215.86 | 8.55 \pm 0.12 | 10.56 | 208.47 | 8.50 \pm 0.10 | 9.84 | 204.69 |
| ImageNet | 16.14 \pm 0.34 | 22.26 | 147.69 | 14.85 \pm 0.27 | 22.62 | 257.45 | 16.44 \pm 0.26 | 19.28 | 145.44 | 17.78 \pm 0.41 | 19.80 | 170.40 | 17.40 \pm 0.33 | 18.87 | 136.91 |
| VGGFace200 | 50.93 \pm 0.86 | 61.43 | 239.61 | 40.78 \pm 0.57 | 96.06 | 478.10 | 109.94 \pm 1.15 | 29.54 | 215.50 | 148.48 \pm 2.87 | 20.70 | 209.86 | 171.31 \pm 3.44 | 15.70 | 127.43 |
| VGGFace500 | 126.19 \pm 1.95 | 23.57 | 162.27 | 150.05 \pm 2.31 | 19.30 | 233.00 | 175.59 \pm 2.46 | 16.74 | 136.21 | 210.75 \pm 1.87 | 12.09 | 130.58 | 182.91 \pm 1.24 | 12.73 | 151.66 |
| Average Rank | 3.5 | 4 | 3 | 4 | 3.75 | 5 | 3.5 | 3.25 | 2.75 | 1.75 | 2.5 | 2.5 | 2.25 | 1.5 | 1.75 |



Figure 3: Samples of VGGFace200. Proj-GAN produces blurry faces. TAC-GAN and P2GAN occasionally show mode collapse (first and last row). The adaptive P2GAN model generates diverse and sharp faces.



Figure 4: Samples of different methods trained on ImageNet. TAC-GAN, f-cGAN and P2GAN all show mode collapse (last two rows), while Proj-GAN and P2GAN-w generate diverse samples.

Mixture of Gaussian (MoG) dataset [6] and evaluate the image generation performance on CIFAR100, ImageNet [39] and VGGFace2 [4]. Following the protocol in [6], we construct 2 subsets VGGFace200 and VGGFace500.

Baselines. We compare our proposed models with competitive baselines including Proj-GAN and TAC-GAN. We use BigGAN [3] as backbone for baselines. For a fair comparison, we implemented TAC-GAN following the paper [6], and we denote as TAC-GAN* in following experiments. The code is written in PyTorch [37] and is available on the

project website[¶].

Evaluation. Inception Scores (IS) [41] and Fréchet Inception Distances (FID) [12] are reported for quantitative evaluation. We compute intra FIDs [30] between the generated images and dataset images within each class. [30] report the mean value of intra FIDs while here we report the maximum among all classes to better capture mode collapse of trained generative models. Experimental setup and additional results are detailed in Supplementary.

[¶]<https://github.com/phymhan/P2GAN>

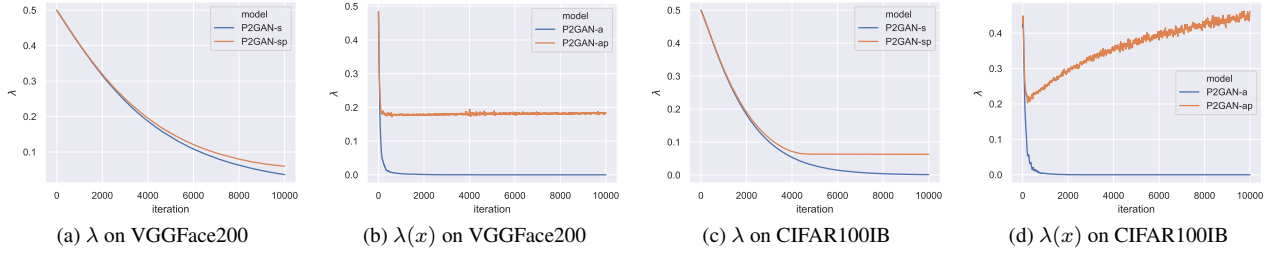


Figure 5: Comparison of scalar λ and amortized $\lambda(x)$. Plots show the value of λ as training proceed. Curves are smoothed for better visualization.

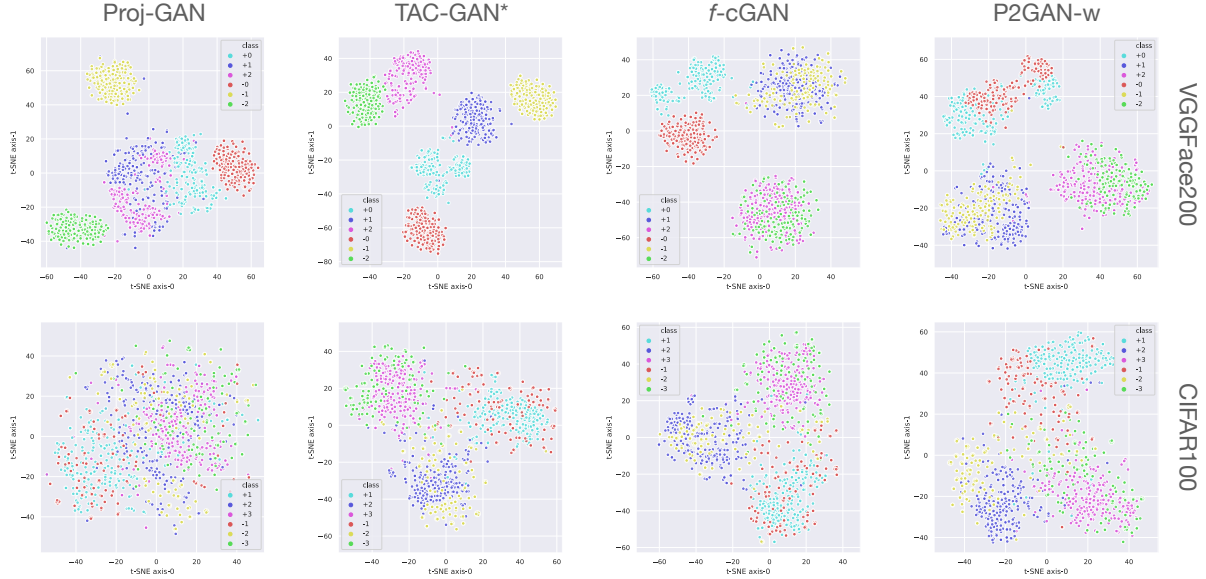


Figure 6: Data embedding visualized by t-SNE. Plot shows 2-D image embedding visualization for baselines at iteration 50000. Positive labels are real image embeddings and negative labels are fake image embeddings. A clear separation between real/fake indicates mode collapse.

Table 5: IS and FID scores on ImageNet at 128 resolution and CIFAR10. We mark '*' to FID and IS values reported in StudioGAN [15].

| | ImageNet 128 × 128 | | CIFAR10 | | |
|--|--------------------|------------------|---------------|------------------|-------------|
| | IS \uparrow | FID \downarrow | IS \uparrow | FID \downarrow | |
| | Proj-GAN | 30.73 | 23.07 | *9.85 | *8.03 |
| | P2GAN | 59.24 | 16.86 | 9.76 | 8.00 |
| | P2GAN-w | 42.69 | 19.19 | 9.87 | 7.99 |

Table 6: Min-LPIPS on VGGFace2 dataset.

| | VGGFace200 | VGGFace500 |
|----------|--------------|--------------|
| Proj-GAN | 0.198 | 0.373 |
| TAC-GAN* | 0.009 | 0.162 |
| f-cGAN | 0.233 | 0.385 |
| P2GAN | 0.172 | 0.376 |
| P2GAN-w | 0.387 | 0.416 |

embeddings are well separated) at iteration 50000. We can also observe that Proj-GAN does not enforce class separability. Moreover, comparing these two datasets, VGGFace is more clustered (in classes) than CIFAR10. This verifies our intuition that when the classification task is relatively easy, enforcing label matching helps the discriminator to be trained more powerful and thus provide more informative

guidance to the generator.

Learning adaptive weights. As shown in Figure 5, without penalty, λ and $\lambda(x)$ quickly converge to 0 during training. Figure 5-(d) shows an interesting phenomenon (from experiments on CIFAR100IB): The model quickly puts high weight on the discrimination loss L_D at the early stage and weighs it less as training proceeds.

f -divergence. Here we consider several commonly used loss functions for f -cGAN and give the training results in Supplementary. We observe that the reverse-KL is the most stable and achieves highest IS and lowest FID. Thus, if not specified, reverse-KL is used in following experiments.

4.2. Comparison of Baselines

Mixture of Gaussian (MoG). We follow protocols in [6] to set up experiments. The real data consists of three 1-D Gaussian with standard deviations $\sigma_0 = 1$, $\sigma_1 = 2$, and $\sigma_2 = 3$, and their means are equally spaced with interval d_m ranging from 1 to 5. Average ranks of Maximum Mean Discrepancy (MMD) [8] are reported in Table 2, where P2GAN achieves highest overall average rank. Detailed MMD metrics are reported in Supplementary. FID scores are reported in Table 3. P2GAN and f -cGAN shows advantages at lower distance values (more overlapping between modes), which suggests that if label matching can be effectively learned (the estimated posteriors are accurate), the discriminator is more powerful.

CIFAR. Results on CIFAR100 [21] are reported in Table 4. Proj-GAN achieves the lowest FID scores, while f -cGAN achieves the highest IS. The adaptive P2GAN model shows competitive high IS and low FID. It is also an interesting confirmation that the P2GAN-w indeed learns a model in between. Results on CIFAR10 are reported in Table 5.

ImageNet. We conduct experiments on ImageNet [39] and compare with all baselines at resolution of 64×64 . From Table 4, we see P2GAN models achieve the highest IS and lowest FID. Intra FIDs are computed on 50 classes (samples of these 50 categories are given in Supplementary) due to its high computation cost. Figure 4 shows that for the “flower” class in the last row, Proj-GAN and the proposed P2GAN-w generate diverse samples, while TAC-GAN, f -cGAN and P2GAN all show mode collapse. This can be verified by low max-FID values of the P2GAN-w model. Results of 128 resolution experiments are reported in Table 5.

VGGFace2. VGGFace2 [4] is a large-scale dataset for face recognition, and contains over 9000 identities with around 362 images for each identity. The VGGFace2 dataset is introduced in [6] for image generation task. We follow their experimental setup and construct subsets VGGFace200 and VGGFace500. The images are resized to 64×64 . Table 4 shows that the proposed f -cGAN and P2GAN models significantly outperform Proj-GAN and TAC-GAN. To directly measure diversity, we report the min-LPIPS (across

all categories) in Table 6. From Figure 3 we can see that Proj-GAN, TAC-GAN and P2GAN all show mode collapse to a certain degree. While P2GAN-w generates sharp and diverse images. Samples from Proj-GAN are also blurry.

4.3. Ablation Studies

A naïve hybrid model could be an ensemble of the Proj-GAN loss and the f -cGAN loss, which requires three parameters v_y , v_y^p and v_y^q . The resulting does not truly untie class embeddings and less elegant. We find it does not show superior performance over dual projection. We provide in Table 7 comparisons of the naïve baseline, an over-parameterization baseline ($\lambda \equiv 0$), and DM-GAN ($\psi \equiv 0$). Also, the training curves on VGGFace200 given in Supplementary shows that over-parameterization alone does not prevent Proj-GAN from failing on this dataset and dual projections indeed benefit from balanced data matching and label matching.

Table 7: FID scores of ablation studies. All models are trained for 60000 iterations on ImageNet, 62000 iterations on CIFAR100, and 50000 iterations on VGGFace200.

| | ImageNet | CIFAR100 | VGGFace200 |
|--------------------|----------|----------|------------|
| Proj-GAN | 24.57 | 10.02 | 61.27 |
| P2GAN | 21.46 | 10.55 | 23.15 |
| $\lambda \equiv 0$ | 23.64 | 10.82 | 62.46 |
| $\psi \equiv 0$ | 26.30 | 10.95 | 87.01 |
| Naïve | - | 10.58 | 32.31 |

5. Conclusion

In this paper, we give insights on projection form of conditional discriminators and propose a new conditional generative adversarial network named Dual Projection GAN (P2GAN). We demonstrate its flexibility in modeling and balancing data matching and label matching. We further rigorously analyze the underlying connections between ACGAN, TAC-GAN, and Proj-GAN. From the analysis, we first propose f -cGAN, a general framework for learning conditional GAN. We demonstrate the efficacy of our proposed models on various synthetic and real-world datasets. P2GAN may also be potentially applicable to image-to-image translation [14, 36] and federated learning [24] which we leave for future work.

Acknowledgments

This research was funded based on partial funding from NSF: IIS 1703883, NSF IUCRC CNS-1747778, CCF-1733843, IIS-1763523, IIS-1849238, and NIH: 1R01HL127661-01 and NIH: R01HL127661-05.

References

[1] Yogesh Balaji, Martin Renqiang Min, Bing Bai, Rama Chellappa, and Hans Peter Graf. Conditional gan with discriminative filter generation for text-to-video synthesis. In *Proceedings of the Twenty-Eighth International Joint Conference on Artificial Intelligence, IJCAI-19*, pages 1995–2001. International Joint Conferences on Artificial Intelligence Organization, 2019. 1

[2] Mohamed Ishmael Belghazi, Aristide Baratin, Sai Rajeswar, Sherjil Ozair, Yoshua Bengio, Aaron Courville, and R Devon Hjelm. Mine: mutual information neural estimation. *arXiv preprint arXiv:1801.04062*, 2018. 2, 4

[3] Andrew Brock, Jeff Donahue, and Karen Simonyan. Large scale gan training for high fidelity natural image synthesis. *arXiv preprint arXiv:1809.11096*, 2018. 1, 6

[4] Qiong Cao, Li Shen, Weidi Xie, Omkar M Parkhi, and Andrew Zisserman. Vggface2: A dataset for recognising faces across pose and age. In *2018 13th IEEE International Conference on Automatic Face & Gesture Recognition (FG 2018)*, pages 67–74. IEEE, 2018. 6, 8

[5] Yunjey Choi, Minje Choi, Munyoung Kim, Jung-Woo Ha, Sunghun Kim, and Jaegul Choo. Stargan: Unified generative adversarial networks for multi-domain image-to-image translation. In *Proceedings of the IEEE conference on computer vision and pattern recognition*, pages 8789–8797, 2018. 1

[6] Mingming Gong, Yanwu Xu, Chunyuan Li, Kun Zhang, and Kayhan Batmanghelich. Twin auxiliary classifiers gan. In *Advances in Neural Information Processing Systems*, pages 1328–1337, 2019. 1, 6, 8, 13, 15

[7] Ian Goodfellow, Jean Pouget-Abadie, Mehdi Mirza, Bing Xu, David Warde-Farley, Sherjil Ozair, Aaron Courville, and Yoshua Bengio. Generative adversarial nets. In *Advances in neural information processing systems*, pages 2672–2680, 2014. 1, 3

[8] Arthur Gretton, Karsten M Borgwardt, Malte J Rasch, Bernhard Schölkopf, and Alexander Smola. A kernel two-sample test. *Journal of Machine Learning Research*, 13(Mar):723–773, 2012. 8

[9] Ligong Han, Ruijiang Gao, Mun Kim, Xin Tao, Bo Liu, and Dimitris Metaxas. Robust conditional gan from uncertainty-aware pairwise comparisons. In *Proceedings of the AAAI Conference on Artificial Intelligence*, volume 34, pages 10909–10916, 2020. 1

[10] Ligong Han, Robert F Murphy, and Deva Ramanan. Learning generative models of tissue organization with supervised gans. In *2018 IEEE Winter Conference on Applications of Computer Vision (WACV)*, pages 682–690. IEEE, 2018. 1

[11] Ligong Han, Anastasis Stathopoulos, Tao Xue, and Dimitris Metaxas. Unbiased auxiliary classifier gans with mine. *arXiv preprint arXiv:2006.07567*, 2020. 2

[12] Martin Heusel, Hubert Ramsauer, Thomas Unterthiner, Bernhard Nessler, and Sepp Hochreiter. Gans trained by a two time-scale update rule converge to a local nash equilibrium. In *Advances in neural information processing systems*, pages 6626–6637, 2017. 6

[13] Judy Hoffman, Eric Tzeng, Taesung Park, Jun-Yan Zhu, Phillip Isola, Kate Saenko, Alexei Efros, and Trevor Darrell. Cycada: Cycle-consistent adversarial domain adaptation. In *International conference on machine learning*, pages 1989–1998. PMLR, 2018. 1

[14] Phillip Isola, Jun-Yan Zhu, Tinghui Zhou, and Alexei A Efros. Image-to-image translation with conditional adversarial networks. In *Proceedings of the IEEE conference on computer vision and pattern recognition*, pages 1125–1134, 2017. 1, 8

[15] Minguk Kang and Jaesik Park. Contragan: Contrastive learning for conditional image generation. 2020. 5, 7, 13, 15

[16] Tero Karras, Timo Aila, Samuli Laine, and Jaakko Lehtinen. Progressive growing of gans for improved quality, stability, and variation. *arXiv preprint arXiv:1710.10196*, 2017. 1

[17] Tero Karras, Miika Aittala, Janne Hellsten, Samuli Laine, Jaakko Lehtinen, and Timo Aila. Training generative adversarial networks with limited data. In *Proc. NeurIPS*, 2020. 4

[18] Alex Kendall, Yarin Gal, and Roberto Cipolla. Multi-task learning using uncertainty to weigh losses for scene geometry and semantics. In *Proceedings of the IEEE conference on computer vision and pattern recognition*, pages 7482–7491, 2018. 2, 4

[19] Diederik P Kingma and Jimmy Ba. Adam: A method for stochastic optimization. *arXiv preprint arXiv:1412.6980*, 2014. 15

[20] Murat Kocaoglu, Christopher Snyder, Alexandros G Dimakis, and Sriram Vishwanath. Causalgan: Learning causal implicit generative models with adversarial training. *arXiv preprint arXiv:1709.02023*, 2017. 2

[21] Alex Krizhevsky, Geoffrey Hinton, et al. Learning multiple layers of features from tiny images. 2009. 5, 8

[22] Chunyuan Li, Hao Liu, Changyou Chen, Yuchen Pu, Liqun Chen, Ricardo Henao, and Lawrence Carin. Alice: Towards understanding adversarial learning for joint distribution matching. In *Advances in Neural Information Processing Systems*, pages 5495–5503, 2017. 4

[23] Yitong Li, Martin Renqiang Min, Dinghan Shen, David E. Carlson, and Lawrence Carin. Video generation from text. In Sheila A. McIlraith and Kilian Q. Weinberger, editors, *Proceedings of the Thirty-Second AAAI Conference on Artificial Intelligence (AAAI-18), New Orleans, Louisiana, USA*, pages 7065–7072. AAAI Press, 2018. 1

[24] Bo Liu, Chaowei Tan, Jiazhou Wang, Tao Zeng, Hua-song Shan, Houpu Yao, Huang Heng, Peng Dai, Liefeng Bo, and Yanqing Chen. Fedlearn-algo: A flexible open-source privacy-preserving machine learning platform. *arXiv preprint arXiv:2107.04129*, 2021. 8

[25] Xuanqing Liu and Cho-Jui Hsieh. Rob-gan: Generator, discriminator, and adversarial attacker. In *Proceedings of the IEEE Conference on Computer Vision and Pattern Recognition*, pages 11234–11243, 2019. 2

[26] Lars Mescheder, Sebastian Nowozin, and Andreas Geiger. Which training methods for gans do actually converge? In *International Conference on Machine Learning (ICML)*, 2018. 4

[27] Mehdi Mirza and Simon Osindero. Conditional generative adversarial nets. *arXiv preprint arXiv:1411.1784*, 2014. 1

[28] Chaitanya Mitash, Bowen Wen, Kostas Bekris, and Abdeslam Boularias. Scene-level pose estimation for multiple instances of densely packed objects. In *Conference on Robot Learning*, pages 1133–1145. PMLR, 2020. 1

[29] Takeru Miyato, Toshiki Kataoka, Masanori Koyama, and Yuichi Yoshida. Spectral normalization for generative adversarial networks. *arXiv preprint arXiv:1802.05957*, 2018. 4

[30] Takeru Miyato and Masanori Koyama. cgans with projection discriminator. *arXiv preprint arXiv:1802.05637*, 2018. 1, 3, 6

[31] Shakir Mohamed and Balaji Lakshminarayanan. Learning in implicit generative models. *arXiv preprint arXiv:1610.03483*, 2016. 1

[32] Youssef Mroueh*, Igor Melnyk*, Pierre Dognin*, Jerret Ross*, and Tom Sercu*. Improved mutual information estimation, 2020. 4

[33] Anh Nguyen, Jeff Clune, Yoshua Bengio, Alexey Dosovitskiy, and Jason Yosinski. Plug & play generative networks: Conditional iterative generation of images in latent space. In *Proceedings of the IEEE Conference on Computer Vision and Pattern Recognition*, pages 4467–4477, 2017. 1

[34] Sebastian Nowozin, Botond Cseke, and Ryota Tomioka. f-gan: Training generative neural samplers using variational divergence minimization. In *Advances in neural information processing systems*, pages 271–279, 2016. 2, 5, 12

[35] Augustus Odena, Christopher Olah, and Jonathon Shlens. Conditional image synthesis with auxiliary classifier gans. In *Proceedings of the 34th International Conference on Machine Learning-Volume 70*, pages 2642–2651. JMLR. org, 2017. 1

[36] Taesung Park, Ming-Yu Liu, Ting-Chun Wang, and Jun-Yan Zhu. Semantic image synthesis with spatially-adaptive normalization. In *Proceedings of the IEEE/CVF Conference on Computer Vision and Pattern Recognition*, pages 2337–2346, 2019. 8

[37] Adam Paszke, Sam Gross, Francisco Massa, Adam Lerer, James Bradbury, Gregory Chanan, Trevor Killeen, Zeming Lin, Natalia Gimelshein, Luca Antiga, et al. Pytorch: An imperative style, high-performance deep learning library. In *Advances in neural information processing systems*, pages 8026–8037, 2019. 6

[38] Scott Reed, Zeynep Akata, Xinchen Yan, Lajanugen Logeswaran, Bernt Schiele, and Honglak Lee. Generative adversarial text to image synthesis. *arXiv preprint arXiv:1605.05396*, 2016. 1

[39] Olga Russakovsky, Jia Deng, Hao Su, Jonathan Krause, Sanjeev Satheesh, Sean Ma, Zhiheng Huang, Andrej Karpathy, Aditya Khosla, Michael Bernstein, et al. Imagenet large scale visual recognition challenge. *International journal of computer vision*, 115(3):211–252, 2015. 2, 3, 6, 8

[40] Mehdi SM Sajjadi, Olivier Bachem, Mario Lucic, Olivier Bousquet, and Sylvain Gelly. Assessing generative models via precision and recall. *arXiv preprint arXiv:1806.00035*, 2018. 15

[41] Tim Salimans, Ian Goodfellow, Wojciech Zaremba, Vicki Cheung, Alec Radford, and Xi Chen. Improved techniques for training gans. In *Advances in neural information processing systems*, pages 2234–2242, 2016. 6

[42] Christian Szegedy, Vincent Vanhoucke, Sergey Ioffe, Jon Shlens, and Zbigniew Wojna. Rethinking the inception architecture for computer vision. In *Proceedings of the IEEE conference on computer vision and pattern recognition*, pages 2818–2826, 2016. 15

[43] Kiran Koshy Thekumparampil, Ashish Khetan, Zinan Lin, and Sewoong Oh. Robustness of conditional gans to noisy labels. *arXiv preprint arXiv:1811.03205*, 2018. 12

[44] Alexandre B Tsybakov. *Introduction to nonparametric estimation*. Springer Science & Business Media, 2008. 12

[45] Han Zhang, Ian Goodfellow, Dimitris Metaxas, and Augustus Odena. Self-attention generative adversarial networks. *arXiv preprint arXiv:1805.08318*, 2018. 1

[46] Han Zhang, Tao Xu, and Hongsheng Li. Stackgan: Text to photo-realistic image synthesis with stacked generative adversarial networks. *2017 IEEE International Conference on Computer Vision (ICCV)*, pages 5908–5916, 2016. 1

[47] Jun-Yan Zhu, Taesung Park, Phillip Isola, and Alexei A Efros. Unpaired image-to-image translation using cycle-consistent adversarial networks. In *Proceedings of the IEEE international conference on computer vision*, pages 2223–2232, 2017. 1

Supplementary

6. Proof of Proposition 1

Proposition 2. When $\psi = 0$, a Proj-GAN reduces to K unconditional GANs, each of them minimizes the Jensen-Shannon divergence between $P_{X|y}$ and $Q_{X|y}$ with mixing ratio $\{\frac{P(y)}{P(y)+Q(y)}, \frac{Q(y)}{P(y)+Q(y)}\}$. Its value function can be written as,

$$\mathbb{E}_{P_Y} \left\{ \mathbb{E}_{P_{X|Y}} \log D(x|y) + \frac{Q_y}{P_y} \mathbb{E}_{Q_{X|Y}} \log (1 - D(x|y)) \right\}.$$

Proof. When $\psi(\cdot)$ is zero, $\tilde{D}(x, y) = v_y^T \phi(x)$. Recall the logit of an unconditional GAN is $\tilde{D}(x) = v_X^T \phi(x)$ (with bias $b = 0$). It immediately follows that matrix V is a collection of K vectors v_y , one for each class. Simply rearranging the cGAN objective, we get

$$\mathbb{E}_{P(y)} \left\{ \mathbb{E}_{P(x|y)} \log D(x|y) + \frac{1}{r(y)} \mathbb{E}_{Q(x|y)} \log (1 - D(x|y)) \right\} \quad (14)$$

with $r(y) = \frac{P(y)}{Q(y)}$. This can be viewed as a weighted sum of K GAN objectives with binary cross-entropy loss. Each of them minimizes the Jensen-Shannon divergence between $P_{X|y}$ and $Q_{X|y}$ with weights $\{\frac{P(y)}{P(y)+Q(y)}, \frac{Q(y)}{P(y)+Q(y)}\}$. \square

7. Proof of Proposition 2

Lemma 1. For any classifier C , the objective $\mathbb{E}_{x,y \sim P_{XY}} \log C(x, y) \leq -H_P(Y|X)$, and the maximizer C^* is obtained if and only if $Q^c(y|x) = P(y|x)$, where Q^c is the conditional distribution induced by C .

Proof. It follows immediately with the observation,

$$\begin{aligned} L_{CE} &= \mathbb{E}_{x,y \sim P_{XY}} \log C(x, y) \\ &= \mathbb{E}_{x \sim P_X} \mathbb{E}_{y \sim P_{Y|X}} \log P(y|x) \frac{Q^c(y|x)}{P(y|x)} \\ &= \mathbb{E}_{x \sim P_X} \mathbb{E}_{y \sim P_{Y|X}} \log P(y|x) - \\ &\quad \mathbb{E}_{x \sim P_X} \text{KL}(P_{Y|X} \| Q^c_{Y|X}) \\ &\leq -H_P(Y|X). \end{aligned} \quad (15)$$

The equality is achieved if and only if $Q^c_{Y|X} = P_{Y|X}$. \square

Proposition 2. Given a generator G , if cross entropy losses L_{mi}^p and L_{mi}^q are minimized optimally, then the difference of two losses evaluated at fake data equals the reverse KL-divergence between $P_{Y|X}$ and $Q_{Y|X}$,

$$L_{mi}^p(x^-) - L_{mi}^q(x^-) = \mathbb{E}_{Q_X} \text{KL}(Q_{Y|X} \| P_{Y|X}). \quad (16)$$

Proof. Applying Lemma 1 to classifier C^p and C^q respectively, we have

$$C^{p*} = P(y|x) \quad \text{and} \quad C^{q*} = Q(y|x). \quad (17)$$

Then,

$$\begin{aligned} &L_{mi}^{p*}(x^-) - L_{mi}^{q*}(x^-) \\ &= \mathbb{E}_{z \sim P_Z, y \sim P_Y} \log Q^{cq*}(G(z, y), y) - \log Q^{cp*}(G(z, y), y) \\ &= \mathbb{E}_{z \sim P_Z, y \sim P_Y} \log \frac{C^{q*}(G(z, y), y)}{C^{p*}(G(z, y), y)} \\ &= \mathbb{E}_{Q_X} \log \frac{Q(y|x)}{P(y|x)} \\ &= \mathbb{E}_{Q_X} \text{KL}(Q_{Y|X} \| P_{Y|X}). \end{aligned}$$

\square

8. Proof of Theorem 1

Theorem 1. Denoting P_{XY} and Q_{XY} as the data distribution and the distribution induced by G , their Jensen-Shannon divergence is upper bounded by the following,

$$\begin{aligned} JSD(P_{XY}, Q_{XY}) &\leq \quad (18) \\ &2c_1 \sqrt{2JSD(P_X, Q_X)} + c_2 \sqrt{2KL(P_{Y|X} \| Q_{Y|X}^p)} + \\ &c_2 \sqrt{2KL(Q_{Y|X} \| Q_{Y|X}^q)} + c_2 \sqrt{2KL(Q_{Y|X}^q \| Q_{Y|X}^p)}. \end{aligned}$$

Proof. According to the triangle inequality of the total variation distance (TV, denoted as δ), we have

$$\delta(P_{XY}, Q_{XY}) \leq \underbrace{\delta(P_{XY}, P_{Y|X}Q_X)}_{(I)} + \underbrace{\delta(P_{Y|X}Q_X, Q_{XY})}_{(II)}. \quad (19)$$

We can relax term (I) using the definition of TV,

$$\begin{aligned} \delta(P_{XY}, P_{Y|X}Q_X) &= \delta(P_{Y|X}P_X, P_{Y|X}Q_X) \\ &= \frac{1}{2} \int \{|P_{Y|X}(y|x)P_X(x) - P_{Y|X}(y|x)Q_X(x)|\mu(x, y)\} \\ &\stackrel{(a)}{\leq} \frac{1}{2} \int |P_{Y|X}(y|x)|\mu(x, y) \int |P_X(x) - Q_X(x)|\mu(x, y) \\ &\leq c_1 \delta(P_X, Q_X), \end{aligned} \quad (20)$$

where μ is a (σ -finite) measure, c_1 is an upper bound of $\int |P_{Y|X}(y|x)|\mu(x, y)$. (a) follows from the Hölder inequality. Similarly, for (II) we have,

$$\begin{aligned} \delta(P_{Y|X}Q_X, Q_{XY}) &= \delta(P_{Y|X}Q_X, Q_{Y|X}Q_X) \\ &\leq c_2 \delta(P_{Y|X}, Q_{Y|X}), \end{aligned} \quad (21)$$

and c_2 is an upper bound of $\int |Q_X(x)|\mu(x)$.

Then, using the triangle inequality of TV again,

$$\begin{aligned} & \delta(P_{Y|X}, Q_{Y|X}) \\ & \leq \delta(P_{Y|X}, Q_{Y|X}^p) + \delta(Q_{Y|X}^p, Q_{Y|X}^q) + \delta(Q_{Y|X}^q, Q_{Y|X}). \end{aligned} \quad (22)$$

Combining Equation 19, 20, 21 and 22,

$$\begin{aligned} & \delta(P_{XY}, Q_{XY}) \\ & \leq c_1 \delta(P_X, Q_X) + c_2 \delta(P_{Y|X}, Q_{Y|X}) \\ & \leq \underbrace{c_1 \delta(P_X, Q_X)}_{\textcircled{III}} + \underbrace{c_2 \delta(Q_{Y|X}^p, Q_{Y|X}^q)}_{\textcircled{IV}} + \\ & \quad \underbrace{c_2 \delta(P_{Y|X}, Q_{Y|X}^p) + c_2 \delta(Q_{Y|X}^q, Q_{Y|X})}_{\textcircled{V}}. \end{aligned} \quad (23)$$

From above, we see that \textcircled{III} is enforced by the unconditional GAN, \textcircled{IV} is minimized by the f -divergence term, and \textcircled{V} is bounded by L_{mi}^p and L_{mi}^q .

Finally, using Pinsker inequality [44] $\delta(P, Q) \leq \sqrt{\frac{1}{2} KL(P\|Q)}$, and Lemma 3 in [43] $\frac{1}{2} \delta^2(P, Q) \leq JSD(P, Q) \leq 2\delta(P, Q)$, we have,

$$\begin{aligned} & JSD(P_{XY}, Q_{XY}) \leq \\ & 2c_1 \sqrt{2JSD(P_X, Q_X)} + c_2 \sqrt{2KL(Q_{Y|X}^q \| Q_{Y|X}^p)} + \\ & c_2 \sqrt{2KL(P_{Y|X} \| Q_{Y|X}^p)} + c_2 \sqrt{2KL(Q_{Y|X} \| Q_{Y|X}^q)}. \end{aligned} \quad (24)$$

□

9. Weighted Dual Projection GAN

P2GAN-ap. The full objectives of P2GAN with amortised weights are as follows,

$$\begin{aligned} L_D^{P2ap} &= \mathbb{E}_{x,y \sim P_{XY}} (1 - \lambda(x)) \mathcal{A}(-\tilde{D}(x, y)) + \\ & \mathbb{E}_{z \sim P_Z, y \sim Q_Y} (1 - \lambda(G(z, y))) \mathcal{A}(\tilde{D}(G(z, y), y)) - \\ & \mathbb{E}_{x,y \sim P_{XY}} \lambda(x) T^p(x, y) - \\ & \mathbb{E}_{z \sim P_Z, y \sim Q_Y} \lambda(G(z, y)) T^q(G(z, y), y) \quad \text{and} \\ L_G^{P2ap} &= \mathbb{E}_{z \sim P_Z, y \sim Q_Y} (1 - \lambda(G(z, y))) \mathcal{A}(-\tilde{D}(G(z, y), y)). \end{aligned} \quad (25)$$

Here T^p and T^q has the same definition as in f -cGAN.

Alternative weighing strategies. An alternative design of a weighted P2GAN is to fix the weight of L_D to 1,

$$L_D^{P2sp-alt} = L_D + \lambda \cdot (L_{mi}^p + L_{mi}^q) - \frac{1}{2} \log \lambda. \quad (26)$$

Here, $\lambda \in [0, \infty)$ and is initialized as 1. We can define similar alternatives for P2GAN-s, P2GAN-a and P2GAN-ap. The key difference is that, weighing $(1 - \lambda) \cdot L_D$ and $\lambda \cdot L_{mi}$ explicitly balances data matching and label matching, while the alternative way balances L_{mi} and the penalty

term. Without penalty, λ in all alternative variants will vanish since this minimizes the total loss, however, the decreasing rate is determined by loss L_{mi} adaptively. An extended comparison is listed in Table 8. In practice, we find the differences are not significant.

Table 8: FID scores of alternative weighting strategies for P2GAN-w. All models are trained for 62000 iterations on CIFAR100 and 50000 iterations on VGGFace200.

| | CIFAR100 | VGGFace200 |
|--------------|-------------|--------------|
| P2GAN-s | 9.03 | 20.59 |
| P2GAN-sp | 9.51 | 20.18 |
| P2GAN-a | 10.13 | 20.26 |
| P2GAN-ap | 9.82 | 18.99 |
| P2GAN-s-alt | 9.49 | 20.21 |
| P2GAN-sp-alt | 9.85 | 20.82 |
| P2GAN-a-alt | 9.98 | 23.25 |
| P2GAN-ap-alt | 9.72 | 21.57 |

10. f -divergence

Here we consider several f -divergence loss functions [34] and list them in Table 9. Results on CIFAR100IB and VGGFace200 is given in Figure 7. Different from the results on VGGFace200, only reverse-KL and GAN losses are stable on CIFAR100IB.

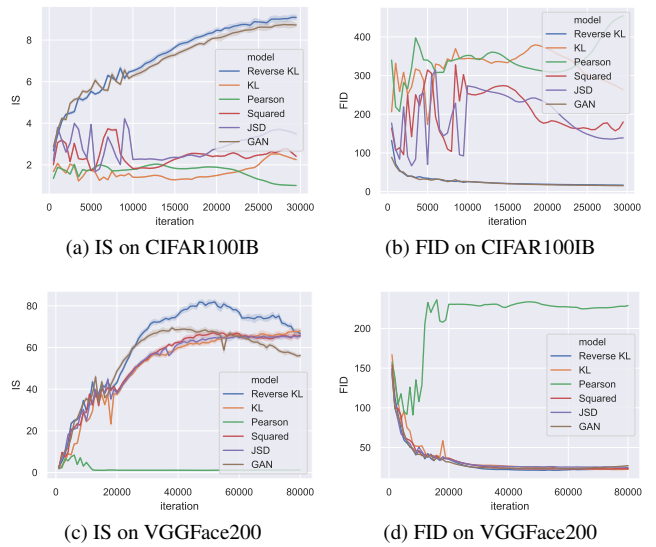


Figure 7: (a-b) IS and FID on CIFAR100IB. (c-d) IS and FID on VGGFace200. Different curves correspond to different choices of f -divergence, CE loss is used for both P and Q .

Table 9: List of f -divergence and their corresponding *generator function* $f(\cdot)$

| Name | $f(u)$ | $f \circ \exp(u)$ |
|--------------------|---|---|
| Reverse KL | $-\log u$ | $-u$ |
| Kullback-leibler | $u \log u$ | ue^u |
| Pearson χ^2 | $(u - 1)^2$ | $(e^u - 1)^2$ |
| Squared Hellinger | $(\sqrt{u} - 1)^2$ | $(e^{u/2} - 1)^2$ |
| Jensen-Shannon GAN | $-(u + 1) \log \frac{1+u}{2} + u \log u$ $u \log u - (u + 1) \log (u + 1)$ | $-(e^u + 1) \log \frac{1+e^u}{2} + ue^u$ $ue^u - (e^u + 1) \log (e^u + 1)$ |

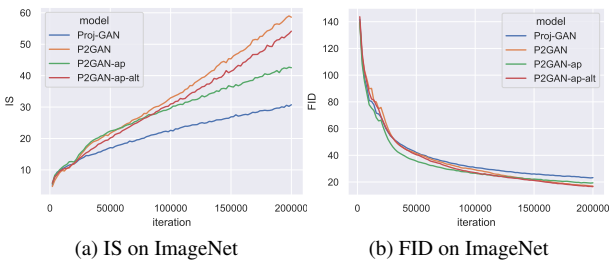


Figure 8: IS and FID score over iterations on ImageNet at at 128×128 resolution.

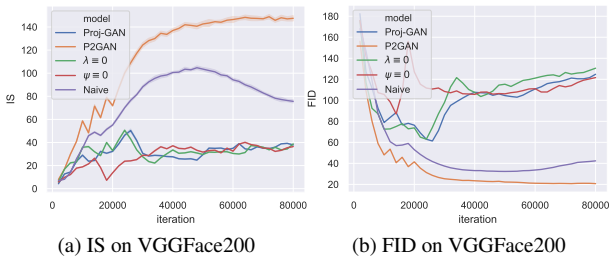


Figure 9: IS and FID score over iterations on VGGFace200.

Table 10: Inception Scores (IS), Fréchet Inception Distances (FID) and the maximum intra FID (max-FID), evaluated on VGGFace200 dataset.

| | IS \uparrow | FID \downarrow | max-FID \downarrow |
|-----------|-------------------------------------|------------------|----------------------|
| Proj-GAN | 50.93 ± 0.86 | 61.43 | 239.61 |
| TAC-GAN* | 40.78 ± 0.57 | 96.06 | 478.10 |
| Naïve | 104.52 ± 1.95 | 32.39 | 196.99 |
| f -cGAN | 109.94 ± 1.15 | 29.54 | 215.50 |
| P2GAN | 148.48 ± 2.87 | 20.70 | 209.86 |
| P2GAN-w | 171.31 ± 3.44 | 15.70 | 127.43 |

11. Implementation

The 1D Mixture of Gaussian experiments are implemented based on the official TAC-GAN repo¹. Code for CIFAR100, VGGFace2, and ImageNet at resolution 64×64 are written based on the BigGAN-PyTorch repo^{**}. Code for CIFAR10 and ImageNet at resolution 128×128 is implemented based on StudioGAN [15] repo^{††}.

12. 1D MoG Synthetic Data

Experimental setup. We follow the same protocol as in TAC-GAN paper [6]. The standard deviations $\sigma_0 = 1$, $\sigma_1 = 2$, and $\sigma_2 = 3$ are fixed, and distance d_m is set to value $1, 2, \dots, 5$ and all models are trained 100 times for each experimental setting. The code for synthetic data, network architectures, and MMD evaluation metrics are borrowed from the official TAC-GAN repo. However, the training code for hinge loss is not provided, thus we implemented our hinge loss version based on the BigGAN-PyTorch repo.

More results. The average MMD values across 100 runs are reported in Table 11 and Figure 10. Samples of generated 1D MoG are visualized in Figure 13. We observe that P2GAN performs the best with BCE loss, demonstrating its ability to generate accurate distributional data. Even with hinge loss, P2GAN still performs relatively well, and achieves the highest overall ranking.

13. CIFAR

Experimental setup. To construct the CIFAR100IB dataset, we randomly sample N_c images from class c where $N_c = \text{round}(500 - 4 \times c)$. For CIFAR100 experiments, we fix batch size as 100, and the number of D steps per G step as 4. All baselines are trained for 500 epochs or 62k iterations. These hyper-parameters are kept the same as described in TAC-GAN paper (also in their provided launch script).

¹<https://github.com/batmanlab/twin-auxiliary-classifiers-gan>

^{**}<https://github.com/ajbrock/BigGAN-PyTorch>

^{††}<https://github.com/POSTECH-CVLab/PyTorch-StudioGAN>

Table 11: The Maximum Mean Discrepancy (MMD) metric on 1D Mixture of Gaussian (MoG) synthetic dataset. Classes ‘0’, ‘1’, ‘2’ stand for mode 0, 1, 2, and ‘M’ stands for marginal. The upper half lists results of BCE loss and the lower half lists results when adopting hinge loss. We run each experiment 100 times and report the average MMD over the top 90% performing runs. Standard deviations are omitted due to space limit. Entries with two lowest values are marked in boldface.

| BCE / Hinge | $d_m = 1$ | | | | $d_m = 2$ | | | | $d_m = 3$ | | | | $d_m = 4$ | | | | $d_m = 5$ | | | |
|----------------|--------------|--------------|--------------|--------------|--------------|--------------|--------------|--------------|--------------|--------------|---------------|--------------|--------------|--------------|---------------|--------------|--------------|--------------|---------------|--------------|
| | 0 | 1 | 2 | M | 0 | 1 | 2 | M | 0 | 1 | 2 | M | 0 | 1 | 2 | M | 0 | 1 | 2 | M |
| Proj-GAN | 0.040 | 0.106 | 0.273 | 0.074 | 0.044 | 0.327 | 1.246 | 0.248 | 0.060 | 0.635 | 1.628 | 0.325 | 0.073 | 0.932 | 3.379 | 0.527 | 0.166 | 3.298 | 3.903 | 1.126 |
| TAC-GAN* | 0.015 | 0.033 | 0.100 | 0.027 | 0.021 | 0.124 | 0.529 | 0.067 | 0.020 | 0.272 | 0.803 | 0.149 | 0.027 | 0.412 | 1.969 | 0.106 | 0.035 | 1.139 | 2.160 | 0.156 |
| <i>f</i> -cGAN | 0.018 | 0.042 | 0.170 | 0.031 | 0.019 | 0.090 | 0.383 | 0.047 | 0.030 | 0.193 | 0.635 | 0.087 | 0.024 | 0.575 | 2.170 | 0.276 | 0.037 | 0.857 | 3.328 | 0.287 |
| P2GAN | 0.009 | 0.028 | 0.151 | 0.026 | 0.014 | 0.080 | 0.345 | 0.046 | 0.016 | 0.160 | 0.639 | 0.084 | 0.028 | 0.237 | 1.530 | 0.056 | 0.030 | 0.655 | 2.725 | 0.261 |
| Proj-GAN | 0.112 | 0.267 | 0.879 | 0.178 | 0.167 | 0.725 | 2.373 | 0.492 | 0.172 | 1.455 | 6.385 | 0.969 | 0.249 | 4.904 | 15.496 | 3.368 | 0.386 | 11.002 | 29.382 | 7.407 |
| TAC-GAN* | 0.190 | 0.474 | 1.376 | 0.416 | 0.304 | 1.635 | 4.213 | 1.060 | 0.357 | 3.504 | 12.817 | 2.531 | 0.314 | 6.949 | 29.822 | 6.425 | 0.264 | 13.905 | 54.134 | 11.125 |
| <i>f</i> -cGAN | 0.164 | 0.429 | 1.484 | 0.441 | 0.192 | 1.718 | 5.084 | 1.506 | 0.174 | 3.480 | 15.491 | 3.675 | 0.138 | 3.629 | 19.597 | 3.862 | 0.173 | 4.592 | 28.753 | 4.315 |
| P2GAN | 0.118 | 0.584 | 1.696 | 0.490 | 0.120 | 0.843 | 4.486 | 1.051 | 0.152 | 2.951 | 12.854 | 2.852 | 0.192 | 6.005 | 22.003 | 5.066 | 0.295 | 9.920 | 36.080 | 8.145 |

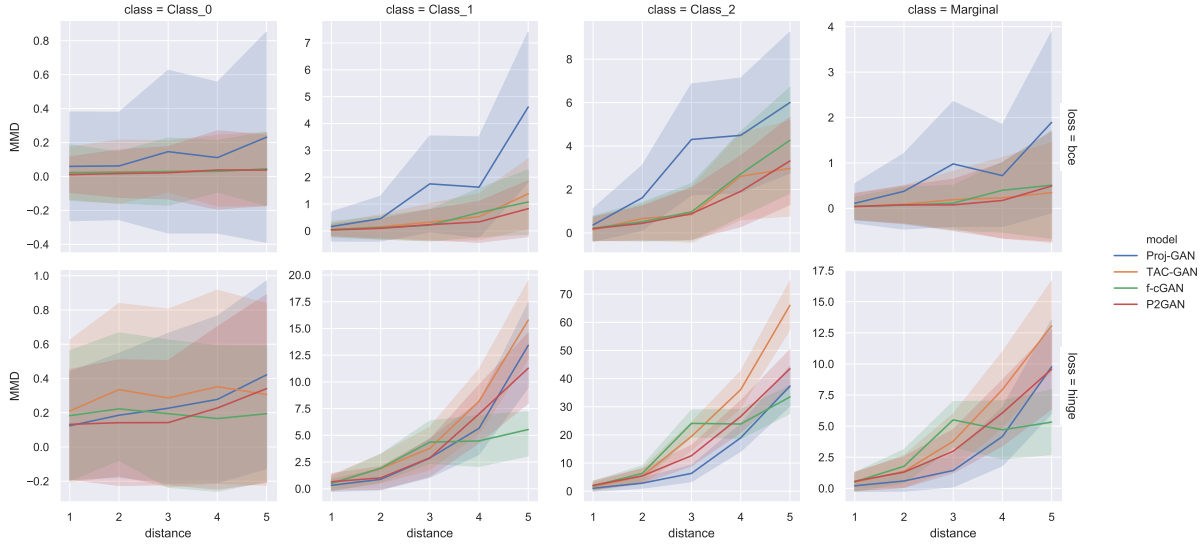


Figure 10: The Maximum Mean Discrepancy (MMD) metric. Proposed methods show low MMD with low variance across different runs.

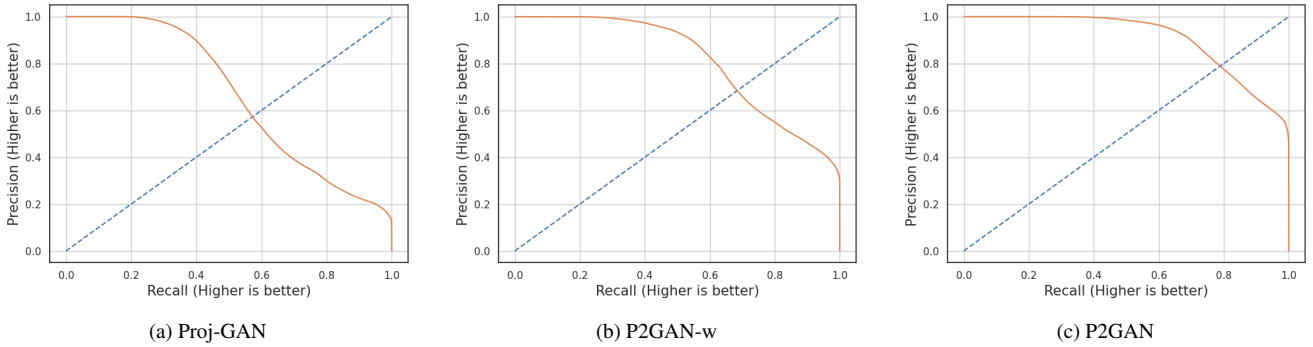


Figure 11: Precision & recall on ImageNet (128 resolution).

More results. Generated samples of CIFAR10 and CIFAR100 are shown in Figure 14 and 16, respectively.

14. ImageNet

Experimental setup. Due to limited computation resource, experiments on ImageNet related to model comparison and

analysis are conducted at resolution 64×64 . We follow the experimental setup in TAC-GAN paper but reduce the image size and model size. We use batch size of 2048 (batch size 256 accumulated 8 times) and the number of D steps per G step is 1. Channel multipliers for both G and D are 32. The resolution of self-attention layer is set to 32. Models are trained with 80k iterations.

For experiments at 128×128 resolution, we follow the configurations of BigGAN256^{††} provided in the StudioGAN [15] repo. We use batch size of 256 and the number of D steps per G step is 2. Channel multipliers for both G and D are 96. The resolution of self-attention layer is set to 64. We train a P2GAN-w model with 200k iterations.

More results. Although P2GAN (without adaptive weights) achieves the highest IS, it shows *mode collapse* on certain classes (for example the “flowers” in row 45). For the same flower class, Proj-GAN can still generate diverse samples. TAC-GAN, f -cGAN and P2GAN all exhibit mode collapse on certain classes. While the proposed weighting strategy is able to avoid mode collapse and still achieve competitively high IS and low FID.

Results of 128×128 resolution ImageNet experiments are reported in Figure 8. The IS and FID curves over training iterations clearly shows its advantage in terms of fast convergence. Precision-recall [40] curves are given in Figure 11. Some randomly generated samples of P2GAN-w during training are shown in Figure 15.

15. VGGFace2

Experimental setup. We follow the same protocol as in TAC-GAN paper, and set batch size to 256 and the number of D steps per G step to 1. Images are resized to resolution of 64×64 . The resolution of self-attention layer is set to 32. Channel multipliers for both G and D are 32. All baselines are trained with 100k iterations.

As for evaluation, we tried our best effort to match the calculated FID and IS with the reported values in TAC-GAN [6]. However, these values can be affected by many factors such as the selected subset of identities and the checkpoint of Inception Net [42] used for evaluation. We first sample a subset of 2000 identities and finetune an Inception model using Adam optimizer [19]. We use the checkpoint at 20000 iteration to monitor the training of GAN models. Then we train a TAC-GAN model^{§§} and select the best model with the lowest FID. Finally, we use the selected TAC-GAN model to examine which Inception Net checkpoint yields the best match. The final FID score is 29.54 which is very close to the reported 29.12. The

^{††}<https://github.com/POSTECH-CVLab/PyTorch-StudioGAN/blob/master/src/configs/ILSVRC2012/BigGAN256.json>

^{§§}Here the model is chosen to be its actual implementation, which is equivalent to f -cGAN with reverse-KL and cross-entropy loss.

identities of subsets VGGFace200, VGGFace500 and VGGFace2000 are given in Supplemental Materials.

More results. As a complementary to the t-SNE visualization of image embeddings provided in the main text, we visualize the samples and list the corresponding FID values in Figure 12. We see that Proj-GAN, TAC-GAN, f -cGAN and P2GAN all show *mode collapse* on identity 0 (the first row) while P2GAN-w still generates diverse samples on the given class. Additional IS and FID values are reported in Table 10.

The training curves of different baselines on VGGFace200 are plotted in Figure 9. We see that Proj-GAN, over-parameterization baseline ($\lambda \equiv 0$), DM-GAN ($\psi \equiv 0$) and the naïve baseline all fail on VGGFace200.

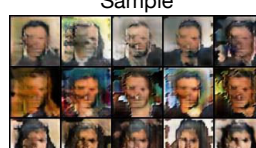
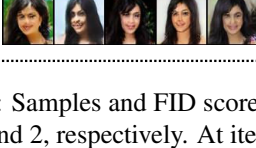
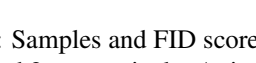
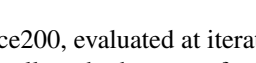
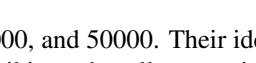
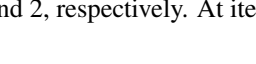
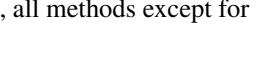
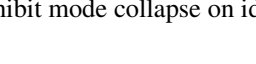
| Proj-GAN | | | TAC-GAN | | | Naive | | |
|------------|---|--------|------------|---|--------|------------|---|--------|
| | Sample | FID | | Sample | FID | | Sample | FID |
| iter 2000 |  | 190.48 | iter 2000 |  | 222.69 | iter 2000 |  | 222.63 |
| |  | 272.70 | |  | 288.47 | |  | 260.91 |
| |  | 227.76 | |  | 288.47 | |  | 242.52 |
| |  | 166.64 | |  | 209.95 | |  | 139.01 |
| |  | 184.80 | |  | 311.72 | |  | 178.42 |
| |  | 177.50 | |  | 253.25 | |  | 125.71 |
| iter 50000 |  | 196.63 | iter 50000 |  | 217.39 | iter 50000 |  | 178.90 |
| |  | 306.88 | |  | 342.89 | |  | 149.23 |
| |  | 223.09 | |  | 210.39 | |  | 80.35 |
| |  | 194.55 | iter 2000 |  | 159.55 | iter 2000 |  | 82.07 |
| |  | 258.16 | |  | 126.44 | |  | 115.76 |
| |  | 213.58 | |  | 83.55 | |  | 65.92 |
| |  | 109.62 | |  | 226.17 | |  | 208.51 |
| |  | 182.49 | |  | 286.70 | |  | 270.50 |
| |  | 122.76 | |  | 229.98 | |  | 225.71 |
| iter 50000 |  | 202.34 | iter 50000 |  | 125.26 | iter 50000 |  | 75.83 |
| |  | 124.08 | |  | 145.91 | |  | 146.47 |
| |  | 88.72 | |  | 113.63 | |  | 112.70 |

Figure 12: Samples and FID scores of VGGFace200, evaluated at iteration 2000, 20000, and 50000. Their identity numbers are 0, 1, and 2, respectively. At iteration 50000, all methods except for P2GAN-w exhibit mode collapse on identity 0.

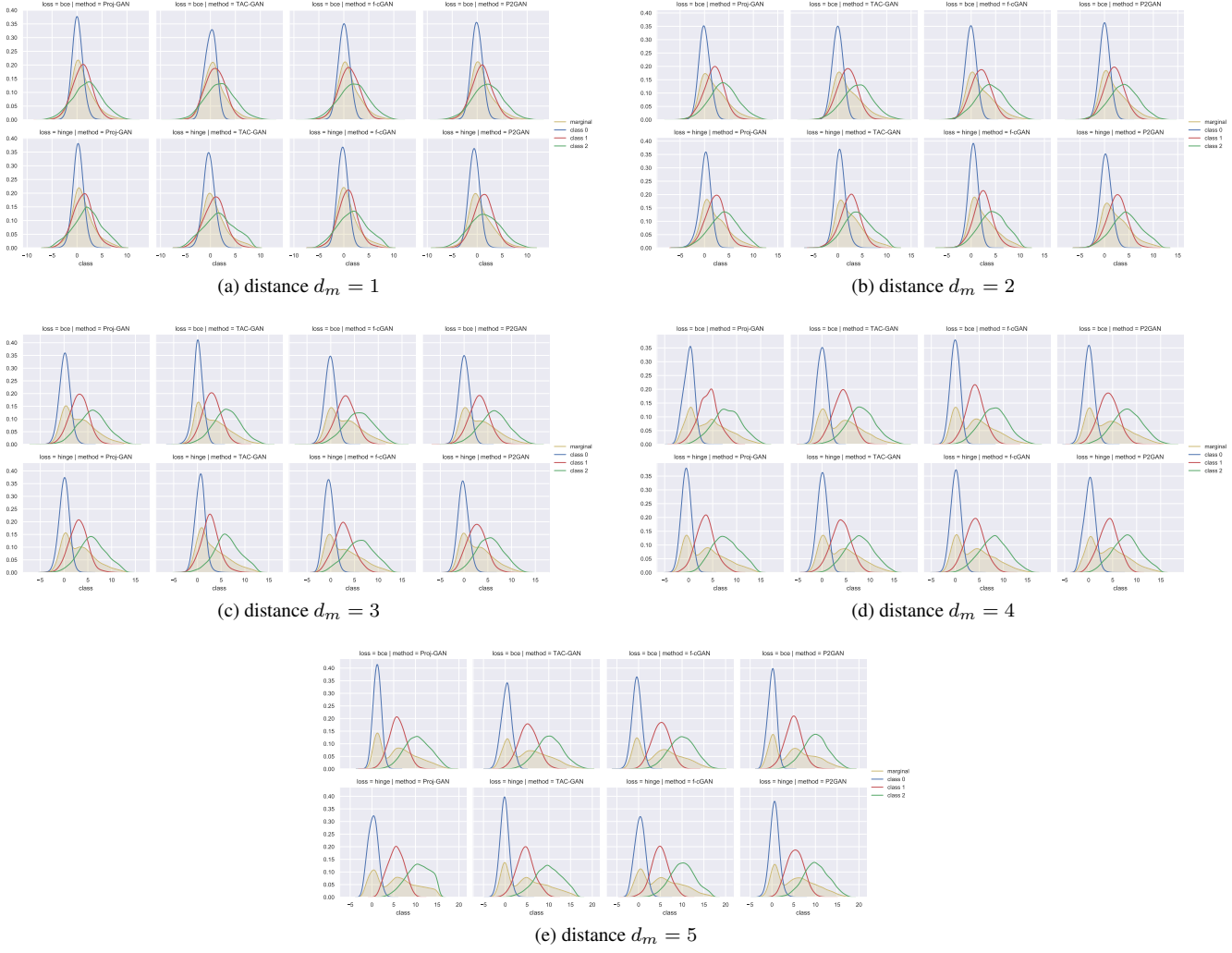
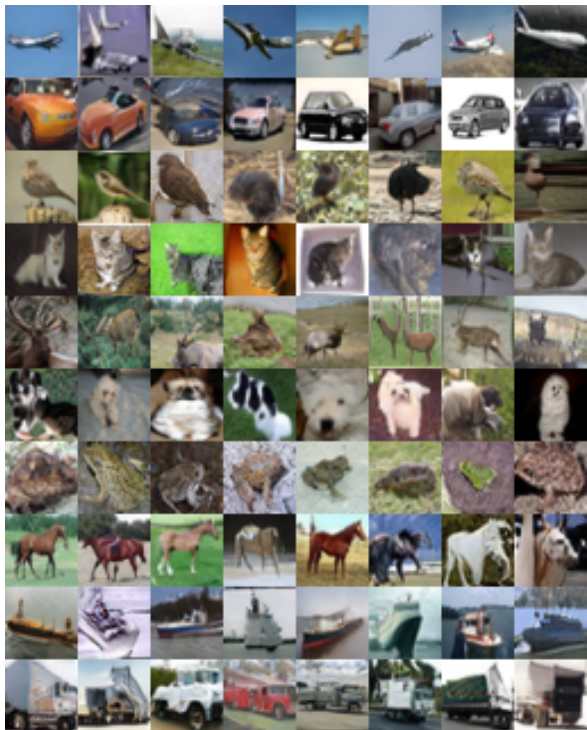
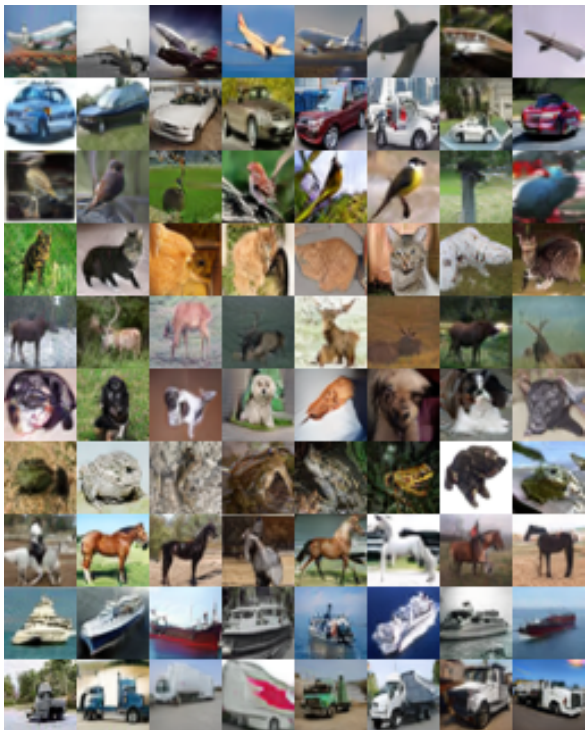


Figure 13: Change distance d_m between the means of adjacent 1-D Gaussian components. For each sub-figure, the first row adopts binary cross entropy loss and the second row adopts hinge loss.



(a) P2GAN



(b) P2GAN-w

Figure 14: 10 classes of CIFAR10 generated samples at 32×32 resolution.

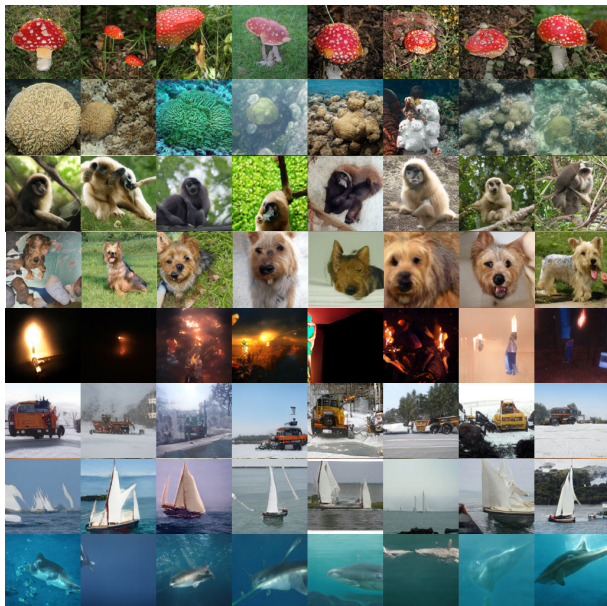
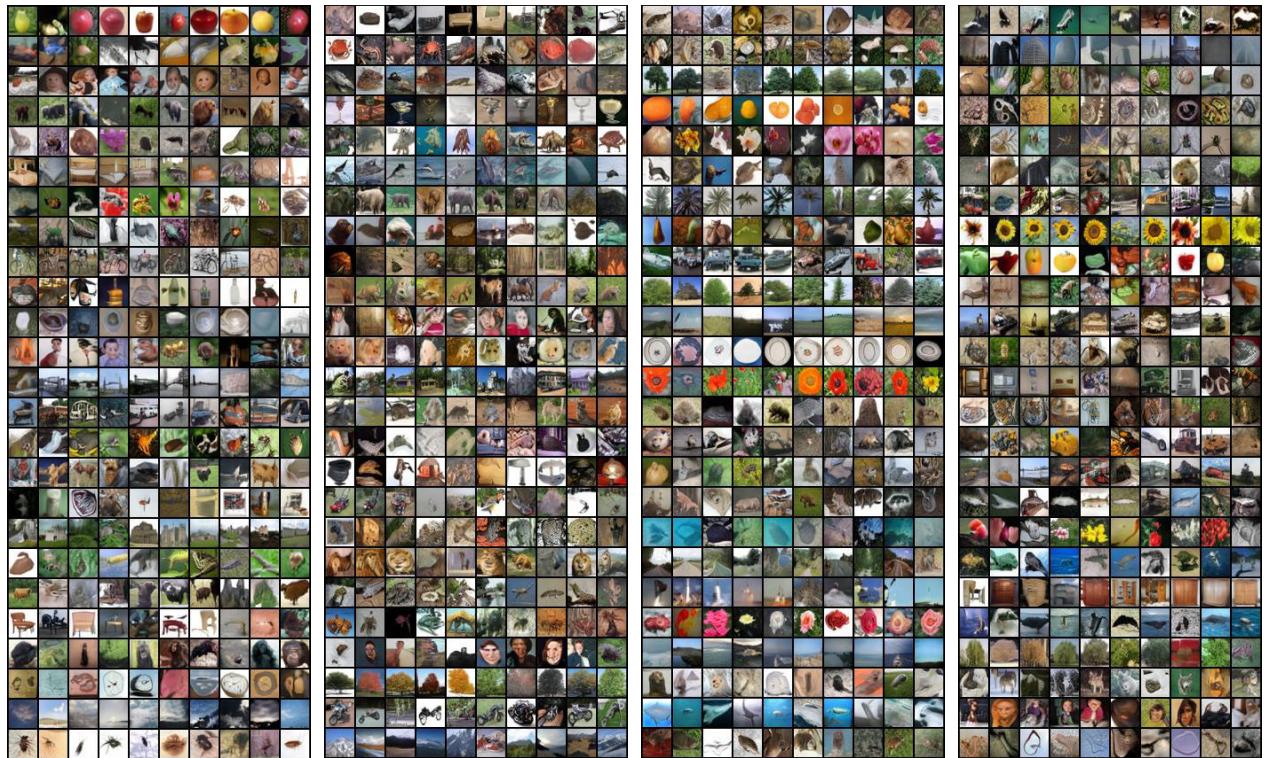


Figure 15: P2GAN-w generated samples on ImageNet at 128×128 resolution.



(a) P2GAN



(b) P2GAN-w

Figure 16: 100 classes of CIFAR100 generated samples at 32×32 resolution.